requirement that the dihedral angle betweeen any two adjacent Se_4^{4-} rectangles be ~45°. The effect of the interchain Se···Se interaction upon the d_{z^2} band structure is found to be appreciable only for those wave vectors along the chain direction (i.e., $\Gamma \rightarrow Z$), which provides a pseudo-one-dimensionality to $(MSe_4)_nI$. Our study also shows that the driving force for the metal ion distortion in the MSe_4 chains diminishes sharply as the d_{z^2} band filling f decreases from $^1/_2$. This is understandable, since the d_{z^2} band orbital at the Fermi level becomes less noded (i.e., more bonding between metal ions) as $f = {}^1/_2 \rightarrow 0$. The apparent absence of a permanent metal ion distortion and the presence of an incommensurate CDW in $(TaSe_4)_2I$ seem to reflect the low band filling (i.e., $f = {}^1/_4$) and the interchain Se···Se interaction.

According to the present study, the **2** → **4a** distortion is as probable as the **2** → **4b** distortion in $(NbSe_4)_3I$. In terms of the lattice strain, the former is expected to be less preferred. Nevertheless, one cannot discount the possibility that the **2** → **4a** distortion can be an alternative to **2** → **4b** at low temperature. For the (1234)-$TaSe_4$ chain, the **2** → **5a** distortion is calculated to have some energy lowering effect. But this distortion is expected to exert significant lattice strain.

Acknowledgment. This work was in part supported by the Camille and Henry Dreyfus Foundation through a Teacher-Scholar Award to M.-H.W., which made it possible for P.G. to visit North Carolina State University. M.-H.W. is grateful to Professor J. K. Burdett for valuable discussion and to Dr. F. J. DiSalvo for information concerning $(MX_4)_nY$ compounds.

Note Added in Proof. A recent X-ray diffraction study of Fujishita et al.[18] on $(MSe_4)_2I$ (M = Nb, Ta) shows that the CDW vector, $2k_f$, along the chain direction is $0.085c^*$, which is equivalent to $0.915c^*$. Our estimate of $2k_f = 0.88c^*$ is in good agreement with this observation.

Registry No. $NbSe_4$, 12034-79-6; $TaSe_4$, 79730-35-1.

(18) Fujishita, H.; Sato, M.; Hoshino, S. *Solid State Commun.* **1984**, *49*, 313.

Contribution from the Department of Chemistry, North Carolina State University, Raleigh, North Carolina 27650, and Laboratoire de Physicochimie des Solides, Université de Nantes, 44072 Nantes Cedex, France

Band Structure of $NbTe_4$

MYUNG-HWAN WHANGBO*[1a,c] and PASCAL GRESSIER[1b]

Received July 22, 1983

Transition-metal tetratelluride chains MTe_4 (M = Nb, Ta) adopt a structure different from that of other tetrachalcogenide chains. Tight-binding calculations on $NbTe_4$ show that multidimensional character is substantially stronger in $NbTe_4$ than in $(MSe_4)_nI$. The $^1/_2$-filled d_{z^2} band of $NbTe_4$ leads to a Fermi surface with two nearly flat pieces, which gives rise to three charge density wave nesting vectors. The band electronic structure of $NbTe_4$ is consistent with the view that in $NbTe_4$ each metal ion Nb^{4+} (d^1) is surrounded by eight Te_2^{2-} dimers.

Chains of general formula MX_4 (M = V, Nb, Ta; X = S, Se, Te) are present in ternary compounds $(MX_4)_nY$ (Y = halogen) and in binary compounds MX_4. These MX_4 chains are found to exhibit two different structures. In the tetraselenides $(MSe_4)_nI$ (M = Nb, Ta),[2] MSe_4 chains are parallel and well separated from one another by iodine atoms. Each metal atom M of an MSe_4 chain is located at the center of an antiprism made up of two *rectangular* Se_4 units as shown in **1**, where the dihedral angle between two adjacent Se_4 units

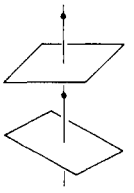

1

is close to 45°. The view of two neighboring Se_4 units projected along the chain axis is shown in **2**. In each Se_4 unit, the

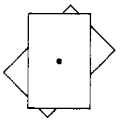

2

shorter Se–Se side (2.35–2.40 Å) is very close to the Se–Se distance of an Se_2^{2-} dimer,[2a,3] while the longer Se–Se side is close to the shortest interchain Se···Se separation. Therefore, each Se_4 rectangle can be considered as made up of two Se_2^{2-} dimers. Thus, if electron removal of iodine atoms is neglected, an MSe_4 chain of $(MSe_4)_nI$ contains an M^{4+} (d^1) ion at the center of every rectangular antiprism of selenium.[2a]

The VS_4 chains present in the binary compound VS_4[4] are found to be isostructural with the MSe_4 chains of $(MSe_4)_nI$. However, this is not the case for the MTe_4 chains of binary compounds MTe_4 (M = Nb, Ta).[5] As shown in the projected view **3a** along the *c* axis, each metal atom of MTe_4 is now located at the center of an antiprism made up of two *square* Te_4 units. It is interesting to consider the formal oxidation state of a metal atom in MTe_4. If each tellurium were to exist as Te^{2-}, there would be no electrons in the d-block bands of MTe_4 and the top portion of the tellurium p-block band should

(1) (a) North Carolina State University. (b) Université de Nantes. (c) Camille and Henry Dreyfus Teacher-Scholar (1980–1985).

(2) (a) Gressier, P.; Whangbo, M.-H.; Meerschaut, A.; Rouxel, J. *Inorg. Chem.*, preceding paper in this issue. (b) Gressier, P.; Meerschaut, A.; Guémas, L.; Rouxel, J.; Monceau, P. *J. Solid State Chem.* **1984**, *51*, 141. (c) Meerschaut, A.; Palvadeau, P.; Rouxel, J. *Ibid.* **1977**, *20*, 21. (d) Guémas, L.; Gressier, P.; Meerschaut, A.; Louer, D.; Grandjean, D. *Rev. Chim. Miner.* **1981**, *18*, 91. (e) Gressier, P.; Guémas, L.; Meerschaut, A. *Acta Crystallogr., Sect. B: Struct. Crystallogr. Cryst. Chem.* **1982**, *38*, 2877. (f) Meerschaut, A.; Gressier, P.; Guémas, L.; Rouxel, J. *J. Solid State Chem.*, in press.

(3) Hodeau, J. L.; Marezio, M.; Roucau, C.; Ayroles, R.; Meerschaut, A.; Rouxel, J.; Monceau, P. *J. Phys. C* **1978**, *11*, 4117.

(4) (a) Allmann, R.; Baumann, L.; Kutoglu, A.; Rösch, H.; Hellner, E. *Naturwissenschaften* **1964**, *51*, 263. (b) Kutoglu, A.; Allmann, R. *Neues Jahrb. Mineral. Monatsh.* **1972**, *8*, 339.

(5) (a) Selte, K.; Kjekshus, A. *Acta Chem. Scand.* **1964**, *18*, 690. (b) Bjerkelund, E.; Kjekshus, A. *J. Less-Common Met.* **1964**, *7*, 231.

0020-1669/84/1323-1228$01.50/0

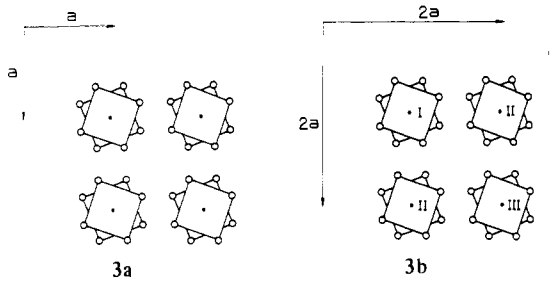

3a 3b

be empty. With square Te_4 units as considered in **3a**, we cannot have such a simple electron-counting scheme as found for the MSe_4 chains. However, it is noted from **3a** that the shortest interchain Te···Te distance (~2.90 Å) is not longer but substantially shorter than the side of a square Te_4 unit (~3.30 Å). This Te···Te distance is comparable in magnitude to the Te–Te distance of Te_2 dimer units in $ZrTe_5$ and $HfTe_5$.[6] Therefore, it seems more reasonable to consider each interchain Te···Te contact as representing a Te_2 dimer. Then the crystal structure of MTe_4 in **3** can be represented as in **4**. In view

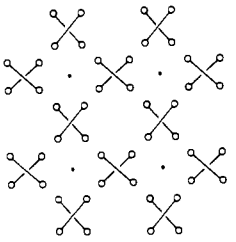

4

of this observation, it seems that MTe_4 compounds should exhibit substantial three-dimensional character. If each Te_2 dimer is counted as a Te_2^{2-} unit, each metal atom in MTe_4 would exist as an M^{4+} (d^1) ion.

X-ray and electron diffraction studies[5,7] on MTe_4 show the presence of superlattice formation, which involves doubling of the *a* axis and tripling of the *c* axis. Thus real MTe_4 with a superlattice consists of four MTe_4 chains per unit cell as shown in **3b**. Recently, Boswell et al. have interpreted the superlattice formation in terms of three charge density waves (CDW's) observed from their electron diffraction study.[7] The wave vectors for these CDW's are $\mathbf{q}_1 \simeq (0, 0, c^*/3)$, $\mathbf{q}_2 \simeq (a^*/2, a^*/2, c^*/3)$, and $\mathbf{q}_3 \simeq (a^*/2, 0, c^*/3)$, where $a^* = 2\pi/a$ and $c^* = 2\pi/c$ with *c* being twice the M–M separation. By analogy with the CDW phenomenon in $NbSe_3$,[8,9] Boswell et al. suggested that MTe_4 contains three slightly different types of MTe_4 chains per unit cell as shown in **3b** (i.e., one type I chain, two type II chains, and one type III chain, which are responsible for the CDW vectors $\mathbf{q}_1$, $\mathbf{q}_2$, and $\mathbf{q}_3$, respectively). CDW formation is typically observed from a low-dimensional material.[10] Thus, MTe_4 compounds appear to have weak three-dimensional character, in contrast to our expectation, based upon its structure in **4**. In order to understand these apparently conflicting observations, we carried out band structure calculations[11] on $NbTe_4$. Molecular and band calculations described in our work are based upon the extended Hückel method.[12] Atomic parameters employed in the present work are listed in Table I.

Table I. The Exponents ζ_μ and the Valence Shell Ionization Potential $H_{\mu\mu}$ for Slater Type Atomic Orbitals χ_μ[a,b]

χ_μ	ζ_μ	ζ_μ'	$H_{\mu\mu}$, eV
Nb 5s	1.9[c]		−10.1
Nb 5p	1.85		−6.86
Nb 4d	4.08 (0.6401)	1.64 (0.5516)	−12.1
Te 5s	2.506[d]		−20.8[e]
Te 5p	2.518		−14.8

[a] The d orbitals of Nb are given as a linear combination of two Slater type orbitals, and each is followed by the weighting coefficient in parentheses. [b] A modified Wolfsberg-Helmholz formula was used to calculate $H_{\mu\nu}$.[16] [c] Reference 17. [d] Reference 18. [e] Reference 19.

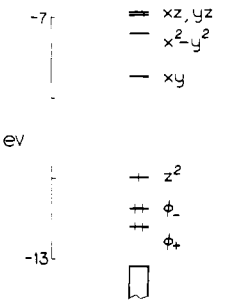

Figure 1. d-block levels of $Nb(Te_2)_8^{12-}$.

Results and Discussion

d-Block Orbitals of $Nb(Te_2)_8^{12-}$. Each metal ion of $NbTe_4$ is surrounded by eight Te_2^{2-} units as discussed in **4**. To probe this local environment of each metal ion, we carried out molecular orbital calculations on the "monomer unit" **5** that

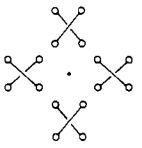

5

contains an Nb^{4+} ion and eight Te_2^{2-} dimers as in **4**. Figure 1 shows the d-block levels of **5** along with some p-block levels lying close to them, where the rectangular block signifies the presence of many closely lying levels of primarily tellurium 5p orbital character. The d_{z^2} level is well separated from the other d-block levels. Except for the ϕ_+ and ϕ_- levels, the d_{z^2} level is also well separated from the p-block orbitals lying below.

The major nodal properties of the ϕ_+ and ϕ_- levels are shown in **6a** and **6b**, respectively. The contribution of tellurium $5p_z$ orbitals, not shown for simplicity, is slightly less than that of tellurium $5p_x$ and $5p_y$ orbitals. The weights of two tellurium 5p orbitals in each Te_2^{2-} dimer are slightly different in **5**. This small difference was neglected in **6**. Note that **5** has two parallel planes of Te_2^{2-} dimers. The in-plane π^* orbitals of

(6) (a) Furuseth, S.; Brattas, L.; Kjekshus, A. *Acta Chem. Scand.* **1973**, *27*, 2367. (b) DiSalvo, F. J.; Fleming, R. M.; Waszczak, J. V. *Phys. Rev. B: Condens. Matter* **1981**, *24*, 2935.
(7) Boswell, F. W.; Prodan, A.; Brandon, J. K. *J. Phys. C* **1983**, *16*, 1067.
(8) (a) Meerschaut, A.; Rouxel, J. *J. Less-Common Met.* **1975**, *39*, 197. (b) Monceau, P.; Ong, N. P.; Portis, A. M.; Meerchaut, A.; Rouxel, J. *Phys. Rev. Lett.* **1976**, *37*, 602. (c) Ong, N. P.; Monceau, P. *Phys. Rev. B: Solid State* **1977**, *16*, 3443. (d) Grüner, G.; Tippie, L. C.; Sanny, J.; Clark, W. C.; Ong, N. P. *Phys. Rev. Lett.* **1980**, *45*, 935. (e) Fleming, R. M.; Grimes, C. C. *Ibid.* **1979**, *42*, 1923. (f) Gill, J. C. *J. Phys. F* **1980**, *10*, 281. (g) Monceau, P.; Richard, J.; Renard, M. *Phys. Rev. B: Condens. Matter* **1982**, *25*, 931. (h) Hodeau, J. L.; Marezio, M.; Roucau, C.; Ayroles, R.; Meerschaut, A.; Rouxel, J.; Monceau, P. *J. Phys. C* **1978**, *11*, 4117. (i) Tsutsumi, K.; Tugagaki, T.; Yamamoto, M.; Shiozaki, Y.; Ido, M.; Sambongi, T.; Yamaya, K.; Abe, Y. *Phys. Rev. Lett.* **1977**, *39*, 1675. (j) Fleming, R. M.; Moncton, D. E.; McWhan, D. B. *Phys. Rev. B: Condens. Matter* **1978**, *18*, 5560.
(9) (a) Wilson, J. A. *Phys. Rev. B: Condens. Matter* **1979**, *19*, 6456. (b) Devreux, F. *J. Phys. (Orsay, Fr.)* **1982**, *43*, 1489. (c) Whangbo, M.-H.; Gressier, P. *Inorg. Chem.* **1984**, *23*, 1305.
(10) (a) Berlinsky, A. J. *Contemp. Phys.* **1976**, *17*, 331. (b) DiSalvo, F. J. "Electron-Phonon Interactions"; Riste, T., Ed.; Plenum Press: New York, 1977; p 107. (c) White, R. M.; Geballe, T. H. "Long Range Order in Solids"; Academic Press: New York, 1979. (d) Whangbo, M.-H. *Acc. Chem. Res.* **1983**, *16*, 95.
(11) (a) Whangbo, M.-H.; Hoffmann, R. *J. Am. Chem. Soc.* **1978**, *100*, 6093. (b) Whangbo, M.-H.; Hoffmann, R.; Woodward, R. B. *Proc. R. Soc. London, Ser. A* **1979**, *366*, 23.
(12) Hoffmann, R. *J. Chem. Phys.* **1963**, *39*, 1397.

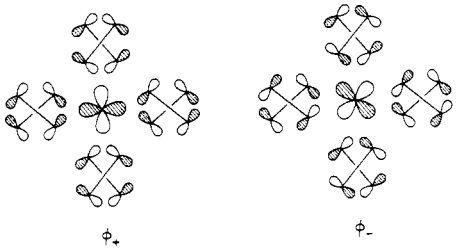

6a 6b

two Te_2^{2-} dimers, lying directly above and below each other, have a bonding interaction in **7a** (π_+*) or antibonding inter-

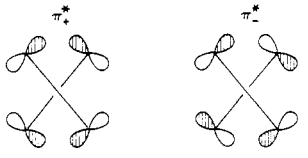

7a 7b

action in **7b** (π_-*). It is the π_+* and π_-* characters that are found in **6a** and **6b**, respectively. By symmetry, $d_{x^2-y^2}$ and d_{xy} orbitals mix into the π* orbitals of Te_2^{2-} dimers as in **6a** and **6b**, respectively, in which the d and π* orbitals are combined in phase. When normalized to a formula unit of $NbTe_4$, **6a** has about 60% tellurium character and **6b** about 50% tellurium character.

With all the levels lying below ϕ_+ doubly occupied, there remain five electrons to fill the ϕ_+, ϕ_-, and d_{z^2} levels. The relative orderings of the ϕ_+, ϕ_-, and d_{z^2} levels depend somewhat upon the valence shell ionization potential (VSIp) of Te 5p. Since the ϕ_+ and ϕ_- levels have more Te 5p character than does the d_{z^2} level, they are more affected by the VSIP of Te 5p. For instance, we found that the ϕ_+ and ϕ_- levels are raised to include the d_{z^2} level between them, when the VSIP of Te 5p is raised by about 2 eV (from −14.8 to −12.8 eV). As will be discussed later, however, the essence of the band electronic structure of $NbTe_4$ around the Fermi level is not strongly affected by the VSIP value of Te 5p.

Band Structure of $NbTe_4$ along $\Gamma \rightarrow Z$. Any two adjacent Te_4 units of a $NbTe_4$ chain are staggered in **3a** so that a unit cell of $NbTe_4$ has the formula $(NbTe_4)_2$. The detailed crystal structure of $NbTe_4$ with superlattice, **3b**, is not known. Thus our band structure calculations on $NbTe_4$ were carried out on the ideal structure **3a**, which consists of only identical $NbTe_4$ chains and therefore has one $NbTe_4$ chain per unit cell. Later in our discussion, we will briefly comment on how the band structure of **3b** could be estimated from that of **3a**. The Brillouin zone[13] for $NbTe_4$ is shown in **8**, where Γ, Z, X, etc.

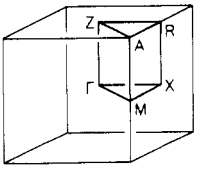

8

are the special points (see Figure 3 caption for details). The d-block band structure of $NbTe_4$ along the chain axis (i.e., Γ → Z) is shown in Figure 2. All the d-block bands are folded since there are two metal ions per unit cell and since each $NbTe_4$ chain has the symmetry element of twofold screw rotation.[2a,11a] This is also the case for the π* band, which results essentially from the ϕ_+ and ϕ_- levels of **5**, since there are two square Te_4 units per unit cell, $(NbTe_4)_2$. The π* and d_{z^2} bands

(13) Lax, M. "Symmetry Principles in Solid State and Molecular Physics"; Wiley: New York, 1974.

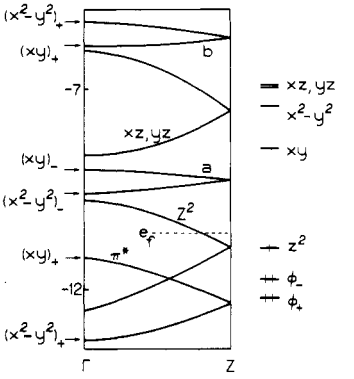

Figure 2. Band structure of $NbTe_4$ along the chain direction Γ → Z in the vicinity of the Fermi level. Symbols such as, for example, $(xy)_+$ and $(xy)_-$ indicate that the band orbitals at Γ have in-phase and out-of-phase combinations of two d_{xy} orbitals within each unit cell. The orbital levels of $Nb(Te_2)_8^{12-}$ are shown on the right-hand side of the chart.

overlap since the ϕ_+ and ϕ_- levels lie close to the d_{z^2} level.

For the purpose of comparison, the ϕ_+, ϕ_- and d-block levels of **5** are shown on the right-hand side of Figure 2. It is clear that the d_{z^2} band is largely derived from the d_{z^2} level and the doubly degenerate $d_{xz,yz}$ band from the doubly degenerate $d_{xz,yz}$ level. In the vicinity of each metal ion, the band orbitals at the top and bottom of the π* band have such nodal properties as shown in **6b** and **6a**, respectively. In addition, the d orbitals in a unit cell combine in phase in the two band orbitals. The two narrow bands a and b, split by about 4 eV, have d_{xy} and $d_{x^2-y^2}$ orbital character as indicated in Figure 2. At Γ, the two metal d orbitals in a unit cell combine out of phase in the band a but in phase in the band b. The out-of-plane π orbitals of two Te_2^{2-} units lying directly above and below each other can be combined in phase as in **9a** (π_+) and out of phase as in **9b**

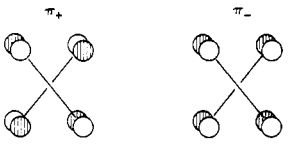

9a 9b

(π_-). In the vicinity of each metal ion, the band orbitals at the bottom and top of the band a are found to have the nodal properties shown in **10a** and **10b**, respectively. Note that **10a**

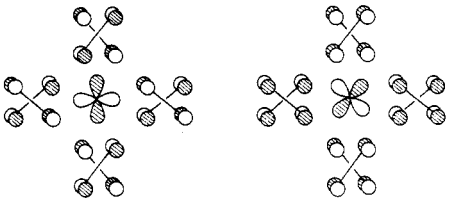

10a 10b

and **10b** have the π_+ and π_- orbital characters, respectively, and that the d and π orbitals combine out of phase in **10**. The band orbitals at the top and bottom of the band b are somewhat complicated. They have contribution from the in plane π* and the σ* orbitals of each Te_2^{2-} dimer. With these orbitals, the metal d orbitals are found to have an antibonding interaction.

Fermi Surface and CDW Vectors. When all the band levels lying below the π* band are completely occupied in Figure 2, six electrons per unit cell are left over to fill the π* and d_{z^2} bands. The Fermi level (i.e., the highest occupied level of a partially filled band) of $NbTe_4$ depends upon how the π* and d_{z^2} bands overlap in the various regions of the Brillouin zone. Figure 3 shows how these two bands vary along some cross

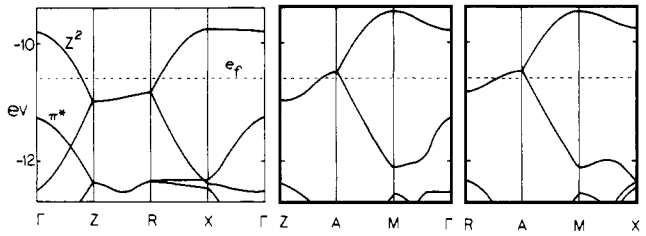

Figure 3. Band structure of $NbTe_4$ along some cross sections of the Brillouin zone, **8**, in the vicinity of the Fermi level. In fractions of the reciprocal vectors a^*, a^*, and c^*, the special points are given as Γ = (0, 0, 0), Z = (0, 0, 0.5), R = (0.5, 0, 0.5), X = (0.5, 0, 0), A = (0.5, 0.5, 0.5), and M = (0.5, 0.5, 0).

sections of the Brillouin zone, where the dashed line represents the Fermi level estimated from the calculated band structure. Note that the Fermi level essentially lies in the d_{z^2} band. The π^* band can be raised, and thus the degree of overlap between the π^* and d_{z^2} bands can be increased, when the VSIP of Te 5p is raised. In order to examine how sensitive the Fermi level is to the VSIP of Te 5p, we performed band structure calculations by varying this value from −14.8 to −12.8 eV. The π^* band is found to be raised upon raising the VSIP of Te 5p, but our calculations show the presence of the Fermi level only in the d_{z^2} band as in Figure 3. Within the wide range of the Te 5p parameters studied, the raising of the π^* band is not high enough to make a hole in the π^* band.

The energy of a band depends upon wave vectors and hence upon the whereabouts of Brillouin zone. The Fermi wave vectors k_f (i.e., those wave vectors giving rise to the Fermi level e_f) of a partially filled band form a surface, which separates those wave vectors leading to the energy above e_f from those leading to the energy below e_f. Such a wave vector surface of a Brillouin zone is known as a Fermi surface.[14] In an understanding of the phenomenon of a CDW formation in a material, knowledge of its Fermi surface is essential. CDW formation is favored when pieces of a Fermi surface satisfy the so-called nesting condition.[10] When two pieces of a Fermi surface are perfectly parallel, all the wave vectors on one piece are obtained from those on the other by simply adding a certain wave vector, **q**. An example of this perfect nesting condition is illustrated in **11**. When two pieces of a Fermi surface are

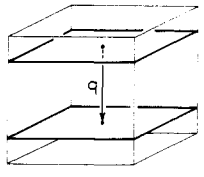

11

not exactly but nearly parallel, most wave vectors on one piece are well approximated by those on the other piece upon adding a certain vector. Thus a CDW formation can occur in such a case as well.

The d_{z^2} band of Figure 3 consists of two subbands. The lower subband is empty in a small region around A, so that a small pocket of hole (i.e., a region of a Brillouin zone leading to unoccupied levels) is found around the eight corners of the Brillouin zone as shown in Figure 4. The upper subband leads to the Fermi surface consisting of two nearly flat pieces shown in Figure 5, where the wave vectors between the two pieces lead to the band energeis above the Fermi level. From our calculations, the centers of the two pieces of the Fermi surface are separated by a wave vector $\mathbf{q}_1^{calcd} \simeq (0, 0, 0.75c^*)$, which is equivalent to $(0, 0, 0.25c^*)$. This is in reasonable agreement

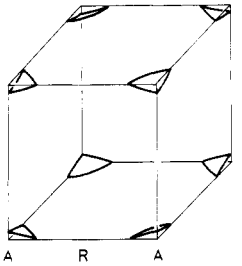

Figure 4. Fermi surface resulting from the lower subband of the d_{z^2} band.

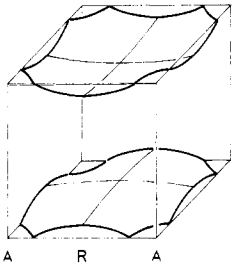

Figure 5. Fermi surface resulting from the upper subband of the d_{z^2} band.

with the experimentally observed value[7] $\mathbf{q}_1 = (0, 0, 0.31c^*)$. Since the two pieces of the Fermi surface are not exactly flat in Figure 5, the wave vector $\mathbf{q}_1^{calcd}$ does not provide a perfect nesting condition. According to the fourfold symmetry of the Fermi surface of Figure 5, it is expected that an approximate nesting condition such as that provided by $\mathbf{q}_1^{calcd}$ can also be obtained from the wave vectors $\mathbf{q}_2^{calcd} \simeq (0.5a^*, 0.5a^*, 0.25c^*)$ and $\mathbf{q}_3^{calcd} \simeq (0.5a^*, 0, 0.25c^*)$. These vectors $\mathbf{q}_2^{calcd}$ and $\mathbf{q}_3^{calcd}$ are close to the experimental values $\mathbf{q}_2 = (0.5a^*, 0.5a^*, 0.34c^*)$ and $\mathbf{q}_3 = (0.5a^*, 0, c^*/3)$, respectively. Slight modification of the ideal $NbTe_4$ chain structure might affect which of the three wave vectors provides the best possible nesting condition.

There are two intrinsic mechanisms by which multiple CDW's can exist in a given compound. One is to have a CDW wave vector with several symmetry-related partners that connect different pieces of the Fermi surface with identical nesting properties. This example is found in many layered compounds such as 2H-$TaSe_2$ and 1T-$TaSe_2$.[15] The Fermi surface of Figure 5 does not allow such a mechanism to operate. The other mechanism is to have several independent pieces of the Fermi surface that support a CDW. For example, $NbSe_3$ contains three different pairs of $NbSe_3$ chains per unit cell,[8,9] two pairs of which give rise to two independent CDW's. Likewise, the Fermi surface of real $NbTe_4$ (**3b**) should have four sets of two nearly flat pieces such as shown in Figure 5, since **3b** contains four $NbTe_4$ chains per unit cell. If these chains are slightly different, so will be the four sets of two nearly flat pieces, thereby leading to three independent CDW's. Thus it seems quite reasonable to consider that different CDW's of MTe_4 are associated with different MTe_4 chains,[7] just as in the case of $NbSe_3$.[9]

Oxidation State of Metal. To rationalize the occurrence of the three CDW vectors $\mathbf{q}_1$, $\mathbf{q}_2$, and $\mathbf{q}_3$ in MTe_4 (M = Nb, Ta), Boswell et al.[7] adapted Wilson's model[9] of CDW formation in $NbSe_3$. They assumed that there exist three types of MTe_4

(14) Ashcroft, N. W.; Mermin, N. D. "Solid State Physics"; Holt, Rinehart and Winston: New York, 1976.

(15) (a) Wilson, J. A.; DiSalvo, F. J.; Mahajan, S. *Adv. Phys.* **1975**, *24*, 117. (b) Mattheiss, L. F. *Phys. Rev. B: Solid State* **1973**, *8*, 3719. (c) DiSalvo, F. J.; Wilson, J. A.; Bagley, B. G.; Waszczak, J. V. *Phys. Rev. B: Solid State* **1975**, *12*, 2220. (d) Haas, C. *Curr. Top. Mater. Sci.* **1979**, *3* (Chapter 1).
(16) Ammeter, J. H.; Bürgi, H.-B.; Thibeault, J. C.; Hoffmann, R. *J. Am. Chem. Soc.* **1978**, *100*, 3686.
(17) Basch, H.; Gray, H. B. *Theor. Chim. Actra* **1966**, *4*, 367.
(18) Clementi, E.; Roetti, C. *At. Data Nucl. Data Tables* **1974**, *14*, 179.
(19) Hinze, J.; Jaffe, H. H. *J. Phys. Chem.* **1963**, *67*, 1501.

chains, and the average number of d electrons per metal is $^2/_3$. In contrast, our electron-counting scheme based upon **4** leads to one d electron per metal ion. In agreement with this counting, the d_{z^2} band of MTe_4 is found to be $^1/_2$ filled in the present calculations. Our study suggests that the three CDW's originate from a Fermi surface consisting of four sets of two nearly flat pieces such as shown in Figure 5. Note from Figure 3 that the energy dispersion of the d_{z^2} band is quite significant along the interchain direction (e.g., Z → A and R → A). It is this kind of substantial interchain interaction that leads to the Fermi surface of Figure 5.

Concluding Remarks

MSe_4 chains of $(MSe_4)_nI$ compounds have each metal ion located at the center of an antiprism made up of two *rectangular* Se_4 units (**2**), where each Se_4 unit can be regarded as consisting of two Se_2^{2-} dimers. However, MTe_4 chains of binary compounds MTe_4 have each metal ion located at the center of an antiprism made up of two *square* Te_4 units (**3**). Unlike the case of MSe_4 chains in $(MSe_4)_nI$,[2a] the shortest interchain Te–Te distance in MTe_4 is *shorter* than the side of a square Te_4 unit within a MTe_4 chain. Consequently, the crystal structure of MTe_4 can be better represented as in **4**, which leads to the view that in MTe_4 each metal ion M^{4+} (d^1) is surrounded by eight Te_2^{2-} dimers. The band structure of MTe_4 shows the presence of a $^1/_2$-filled d_{z^2} band that gives rise to the Fermi surface with two nearly flat pieces (Figure 5). From such a Fermi surface, one can derive three CDW nesting vectors, which are in reasonable agreement with experiment. Our study shows that multidimensional character is much stronger in MTe_4 than in $(MSe_4)_nI$.

Acknowledgment. This work was in part supported by the Camille and Henry Dreyfus Foundation through a Teacher-Scholar Award to M.-H.W., which made it possible for P.G. to visit North Carolina State University. We are thankful to Drs. A. Meerschaut and P. Monceau for references and valuable comments. M.-H.W. is especially grateful to Dr. F. J. DiSalvo for his critical comments concerning two intrinsic mechanisms of multiple CDW's and to Professor F. W. Boswell for valuable discussion on $NbTe_4$ and $TaTe_4$.

Registry No. $NbTe_4$, 12034-85-4.

Contribution from Lawrence Berkeley Laboratory, University of California, Berkeley, California 94720, and Department of Chemistry, Seton Hall University, South Orange, New Jersey 07079

Photophysical Studies of Uranyl Complexes. 4. X-ray Photoelectron and Luminescence Studies of Hydrolyzed Uranyl Salts

DALE L. PERRY,*† LEON TSAO, and HARRY G. BRITTAIN‡

Received September 30, 1983

The solid-state hydrolysis products of uranyl ion, UO_2^{2+}, have been studied with use of X-ray photoelectron and luminescence spectroscopy. The products, consisting of uranium oxides and various forms of uranyl hydroxide, gave "averaged" uranium 4f photoelectron binding energies of 381.5–381.8 eV and oxygen 1s binding energies of 530.8–531.9 eV. Evidence for carbon dioxide chemisorption from the atmosphere was observed by monitoring the carbon 1s line for samples that had been exposed to the atmosphere for extended periods of time. The luminescence spectra of all sets of hydrolysis products were essentially identical, consisting of two well-defined, broad peaks at 10 K. The luminescence lifetimes of each pair of bands were found to be identical within experimental error. A lifetime of 100–115 μs was observed for most samples, yielding a ground-state vibrational energy of 700–730 cm^{-1}. For other products, the emission lifetimes were significantly smaller, giving ground-state vibrational energies of less than 700 cm^{-1} and implying that counterion interactions were operable in several of the hydrolysis product mixtures.

Introduction

The solid-state hydrolysis products of uranium have been the subject of several studies. The compounds, formed by the hydrolysis of uranyl salts by bases such as sodium and ammonium hydroxide, exhibit variable chemical compositions that are heavily dependent on the method of preparation. Parameters that have been shown to affect these compositions include aging of the precipitates under carefully controlled conditions approaching equilibrium,[1] temperature,[2] or pressure[3] experienced by several forms of the solid hydrolysis precipitates, and the hydroxide/uranium ratio used.[1] As a result, not only are different chemical compositions formulated for these compounds (among them, $Na_2O{\cdot}8UO_3$,[4] $Na_2U_7O_{22}$ (uranates),[1] $U_3O_8(OH)_2$,[5] and $3UO_3{\cdot}NH_3{\cdot}5H_2O$[6]), but also mixtures of various pure compounds almost always result in these precipitates. The chemistry of many of the compounds in these hydrolysis product mixtures has been discussed extensively in a review,[7] however, and several have been structurally documented as being true uranyl hydroxides; uranium oxides have also been shown to be present in the mixture of hydrolysis products.[5]

The present study is one that further attempts to obtain a clear and more complete picture of the chemistry of this mixture of compounds that comprise the hydrolysis products of the uranyl ion. By the use of both X-ray photoelectron and luminescence spectroscopy, along with other characterizational techniques such as energy dispersive X-ray and infrared spectroscopy, mass spectrometry, and scanning electron microscopy, a more complete physical chemistry and analytical picture of the aqueous hydrolysis products can be obtained.

Experimental Section

Because of the rather large number of compounds and compound mixtures produced by varying the preparative procedure, two standard sets of products were prepared and used for all measurements for the present study. First, two different concentrations of the uranyl ion solution being hydrolyzed were used in order to determine if there was any initial uranyl ion solution concentration dependence on the

† University of California.
‡ Seton Hall University

(1) Wamser, C. A.; Belle, J.; Bernsohn, E.; Williamson, B. J. *J. Am. Chem. Soc.* **1952**, *74*, 1029.
(2) Taylor, J. C. *Acta Crystallogr., Sect. B: Struct. Crystallogr. Cryst. Chem.* **1971**, *B27*, 1088.
(3) Debets, P. C.; Loopstra, B. O. *J. Inorg. Nucl. Chem.* **1963**, *25*, 945.
(4) Guiter, H. *Bull. Soc. Chim. Fr.* **1947**, 275.
(5) Hoekstra, H. R.; Siegel, S. *J. Inorg. Nucl. Chem.* **1973**, *35*, 761.
(6) Cordfunke, E. H. P. *J. Inorg. Nucl. Chem.* **1962**, *24*, 303.
(7) Berg, L.; Heibel, B.; Hinz, I.; Karl, W.; Keller-Rudek, H.; Leonard, A.; Reprecht, S.; Stiess, P. "Gmelin Handbuch der Anorganischen Chemie"; Springer-Verlag: Berlin, 1978; Uranium Suppl. Vol. C2.

0020-1669/84/1323-1232$01.50/0